ered the effects of buoyancy in the case of inclined, continuous moving sheets. But in nature, along with the free convection currents, the flow is also caused by the differences in concentration or material constitution, e.g., The atmospheric flows. The effects of mass transfer of the flow past an infinite vertically moving plate were studied by Soundalgekar [7]. Ganesan & Muthukumaraswamy [8] analyzed an unsteady flow past an impulsively started semi-infinite vertical plate with heat and mass transfer by implicit finite difference scheme.

In literature only very few authors studied the flow past semi-infinite vertical cylinder. Yang [9] made a study of unsteady laminar free convection on vertical plates and cylinders to establish necessary and sufficient conditions under which similarity solutions are possible. On the basis of these conditions, all possible cases are derived including those for unsteady conditions. Bottemanne [10] studied the combined effect of heat and mass transfer in the steady laminar boundary layer of a vertical cylinder placed in still air. Minkowycz & Sparrow [11] used local velocity and temperature profiles for isothermal cylinder placed in air.

In the process of manufacturing glass or polymer fibers, filaments of hot materials are extruded through a circular orifice. They are cooled as they pass through the surrounding environment. A fiber can be regarded as a continuous infinite circular cylinder issuing into the fluid of infinite extent. Several authors have analysed the flows generated by continuously moving surfaces. Badr & Dennis [12] carried out a time dependent viscous flow past an impulsively started rotating and translating circular cylinder. The cooling of fibres in the formation process was studied by Bourne & Dixon [13]. In the investigation the effect of buoyancy force was neglected. Collins & Dennis [14] made a numerical method of expansion in powers of the time for an impulsively started circular cylinder by using an implicit time-dependent numerical integration procedure. They [15] are also studied symmetrical flow past a uniformly accelerated circular cylinder.

But the effects of buoyancy forces on flow over an impulsively moving semi-infinite vertical cylinder with heat and mass transfer has not received the attention of any researcher. In many industrial applications, the flow past a moving semi-infinite vertical cylinder plays an important role. Here, intrusive may be taken as an isothermal vertical cylinder with impulsive motion subjected to uniform concentration. It is now proposed to study the effects of heat and mass transfer on the natural convection flow of an incompressible viscous fluid past a semi-infinite isothermal vertical cylinder using an implicit finite difference scheme.

2
Mathematical analysis

Consider the free convection flow of a viscous incompressible, laminar flow over an impulsively moving semi-infinite vertical cylinder of radius r_0. Initially both cylinder and the fluid are stationary at the same temperature T'_∞ and also at the same concentration level C'_∞. At a time $t' \geq 0$, the cylinder starts moving in the vertical direction with velocity u_0. The temperature and concentration on the surface of the cylinder are also raised to T'_w and C'_w. The effect of viscous dissipation is assumed to be negligible. The axis and radial co-ordinates are taken to be x and r, with x-axis measured vertically upward along the axis of the cylinder and r-axis measured normal to axis of cylinder. Under these assumptions, the governing boundary layer equations of continuity, momentum, energy and species concentration with Boussinesq's approximation are as follows:

$$\frac{\partial(ru)}{\partial x} + \frac{\partial(rv)}{\partial r} = 0 \tag{1}$$

$$\frac{\partial u}{\partial t'} + u\frac{\partial u}{\partial x} + v\frac{\partial u}{\partial r} = g\beta(T' - T'_\infty) + g\beta^*(C' - C'_\infty) + \frac{\upsilon}{r}\frac{\partial}{\partial r}\left(r\frac{\partial u}{\partial r}\right) \tag{2}$$

$$\frac{\partial T'}{\partial t'} + u\frac{\partial T'}{\partial x} + v\frac{\partial T'}{\partial r} = \frac{\alpha}{r}\frac{\partial}{\partial r}\left(r\frac{\partial T'}{\partial r}\right) \tag{3}$$

$$\frac{\partial C'}{\partial t'} + u\frac{\partial C'}{\partial x} + v\frac{\partial C'}{\partial r} = \frac{D}{r}\frac{\partial}{\partial r}\left(r\frac{\partial C'}{\partial r}\right) \tag{4}$$

The initial and boundary conditions are

$$\begin{aligned} t' \leq 0: &\quad u = 0,\ v = 0,\ T' = T'_\infty,\ C' = C'_\infty \text{ for all } x \text{ and } r \\ t' > 0: &\quad u = u_0,\ v = 0,\ T' = T'_w,\ C' = C'_w \text{ at } r = r_0 \\ &\quad u = 0,\ T' = T'_\infty,\ C' = C'_\infty \text{ at } x = 0 \text{ and } r \geq r_0 \\ &\quad u \to 0,\ T' \to T'_\infty,\ C \to C'_\infty \text{ as } r \to \infty \end{aligned} \tag{5}$$

Introducing the following non-dimensional quantities

$$X = \frac{x\nu}{u_0 r_0^2},\quad R = \frac{r}{r_0},\quad U = \frac{u}{u_0},\quad V = \frac{vr_0}{\upsilon},\quad t = \frac{t'\nu}{r_0^2},$$

$$T = \frac{T' - T'_\infty}{T'_w - T'_\infty},\quad C = \frac{C' - C'_\infty}{C'_w - C'_\infty},\quad \mathrm{Gr} = \frac{g\beta r_0^2(T'_w - T'_\infty)}{\upsilon u_0},$$

$$\mathrm{Gc} = \frac{g\beta^* r_0^2(C'_w - C'_\infty)}{\upsilon u_0},\quad \mathrm{Sc} = \frac{\upsilon}{D},\quad \mathrm{Pr} = \frac{\upsilon}{\alpha}, \tag{6}$$

Eqs. (1)–(4) are reduced to the following form:

$$\frac{\partial(RU)}{\partial X} + \frac{\partial(RV)}{\partial R} = 0 \tag{7}$$

$$\frac{\partial U}{\partial t} + U\frac{\partial U}{\partial X} + V\frac{\partial U}{\partial R} = \mathrm{Gr}T + \mathrm{Gc}C + \frac{1}{R}\frac{\partial}{\partial R}\left(R\frac{\partial U}{\partial R}\right) \tag{8}$$

$$\frac{\partial T}{\partial t} + U\frac{\partial T}{\partial X} + V\frac{\partial T}{\partial R} = \frac{1}{\mathrm{Pr}R}\frac{\partial}{\partial R}\left(R\frac{\partial T}{\partial R}\right) \tag{9}$$

$$\frac{\partial C}{\partial t} + U\frac{\partial C}{\partial X} + V\frac{\partial C}{\partial R} = \frac{1}{\mathrm{Sc}R}\frac{\partial}{\partial R}\left(R\frac{\partial C}{\partial R}\right) \tag{10}$$

The corresponding initial and boundary conditions in non-dimensional quantities are given by

$$
\begin{aligned}
&t \le 0: \quad U = 0, \quad V = 0, \quad T = 0, \quad C = 0 \text{ for all } X \text{ and } R \\
&t > 0: \quad U = 1, \quad V = 0, \quad T = 1, \quad C = 1 \text{ at } R = 1 \\
&\qquad\quad U = 0, \quad T = 0, \quad C = 0 \text{ at } X = 0 \\
&\qquad\quad U \to 0, \quad T \to 0, \quad C \to 0 \text{ as } R \to \infty
\end{aligned} \tag{11}
$$

3
Numerical technique

In order to solve the unsteady, non-linear coupled Eqs. (7)–(10) under the condition (11), an implicit finite difference scheme of Crank–Nicolson type has been employed. The region of integration is considered as a rectangle with sides $X_{\max}(= 1.0)$ and $R_{\max}(= 20.0)$ where $R_{\max}$ corresponds to $R = \infty$ which lies very well outside the momentum, thermal and concentration boundary layers. Appropriate mesh sizes $\Delta X = 0.02$, $\Delta R = 0.25$ and time step $\Delta t = 0.01$ are considered for calculations. The finite-difference equations corresponding to Eqs. (7)–(10) are as follows:

$$
\begin{aligned}
&\frac{U^{m+1}_{i,j-1} - U^{m+1}_{i-1,j-1} + U^{m+1}_{i,j} - U^{m+1}_{i-1,j} + U^{m}_{i,j-1} - U^{m}_{i-1,j-1} + U^{m}_{i,j} - U^{m}_{i-1,j}}{4\Delta X} \\
&\quad + \frac{V^{m+1}_{i,j} - V^{m+1}_{i,j-1} + V^{m}_{i,j} - V^{m}_{i,j-1}}{2\Delta R} + \frac{V^{m+1}_{i,j}}{1 + (j-1)\Delta R} = 0
\end{aligned} \tag{12}
$$

$$
\begin{aligned}
&\frac{U^{m+1}_{i,j} - U^{m}_{i,j}}{\Delta t} + \frac{U^{m}_{i,j}}{2\Delta X}\left(U^{m+1}_{i,j} - U^{m+1}_{i-1,j} + U^{m}_{i,j} - U^{m}_{i-1,j}\right) \\
&+ \frac{V^{m}_{i,j}}{4\Delta R}\left(U^{m+1}_{i,j+1} - U^{m+1}_{i,j-1} + U^{m}_{i,j+1} - U^{m}_{i,j-1}\right) \\
&\quad = \mathrm{Gr}\frac{T^{m+1}_{i,j} + T^{m}_{i,j}}{2} + \mathrm{Gc}\frac{C^{m+1}_{i,j} + C^{m}_{i,j}}{2} \\
&\qquad + \frac{\left(U^{m+1}_{i,j-1} - 2U^{m+1}_{i,j} + U^{m+1}_{i,j+1} + U^{m}_{i,j-1} - 2U^{m}_{i,j} + U^{m}_{i,j+1}\right)}{2(\Delta R)^2} \\
&\qquad + \frac{\left(U^{m+1}_{i,j+1} - U^{m+1}_{i,j-1} + U^{m}_{i,j+1} - U^{m}_{i,j-1}\right)}{4[1 + (j-1)\Delta R]\Delta R}
\end{aligned} \tag{13}
$$

$$
\begin{aligned}
&\frac{T^{m+1}_{i,j} - T^{m}_{i,j}}{\Delta t} + \frac{U^{m}_{i,j}}{2\Delta X}\left(T^{m+1}_{i,j} - T^{m+1}_{i-1,j} + T^{m}_{i,j} - T^{m}_{i-1,j}\right) \\
&+ \frac{V^{m}_{i,j}}{4\Delta R}\left(T^{m+1}_{i,j+1} - T^{m+1}_{i,j-1} + T^{m}_{i,j+1} - T^{m}_{i,j-1}\right) \\
&\quad = \frac{\left(T^{m+1}_{i,j-1} - 2T^{m+1}_{i,j} + T^{m+1}_{i,j+1} + T^{m}_{i,j-1} - 2T^{m}_{i,j} + T^{m}_{i,j+1}\right)}{2\mathrm{Pr}(\Delta R)^2} \\
&\qquad + \frac{\left(T^{m+1}_{i,j+1} - T^{m+1}_{i,j-1} + T^{m}_{i,j+1} - T^{m}_{i,j-1}\right)}{4\mathrm{Pr}[1 + (j-1)\Delta R]\Delta R}
\end{aligned} \tag{14}
$$

$$
\begin{aligned}
&\frac{C^{m+1}_{i,j} - C^{m}_{i,j}}{\Delta t} + \frac{U^{m}_{i,j}}{2\Delta X}\left(C^{m+1}_{i,j} - C^{m+1}_{i-1,j} + C^{m}_{i,j} - C^{m}_{i-1,j}\right) \\
&\quad + \frac{V^{m}_{i,j}}{4\Delta R}\left(C^{m+1}_{i,j+1} - C^{m+1}_{i,j-1} + C^{m}_{i,j+1} - C^{m}_{i,j-1}\right) \\
&\quad = \frac{\left(C^{m+1}_{i,j-1} - 2C^{m+1}_{i,j} + C^{m+1}_{i,j+1} + C^{m}_{i,j-1} - 2C^{m}_{i,j} + C^{m}_{i,j+1}\right)}{2\mathrm{Sc}(\Delta R)^2} \\
&\qquad + \frac{\left(C^{m+1}_{i,j+1} - C^{m+1}_{i,j-1} + C^{m}_{i,j+1} - C^{m}_{i,j-1}\right)}{4\mathrm{Sc}[1 + (j-1)\Delta R]\Delta R}
\end{aligned} \tag{15}
$$

Here i-designates X-direction $i\Delta X$, j-designates R-direction $1 + (j-1)\Delta R$ and the superscript m designates a value of time $m\Delta t$. During any one-time step, the coefficients $U^{m}_{i,j}$ and $V^{m}_{i,j}$ appearing in Eq. (12)–(15) are treated as constants. The values of U, V, T and C are known at time $t = 0$ from the initial conditions. The values of C, T, V and U at the next time step $t = \Delta t$ are calculated as follows:

Equation (15) at every internal nodal point on a particular i-level constitute a tri-diagonal system of equations which is solved by Thomas algorithm, described by Carnahan et al. [16]. Thus, the values of C are known at every nodal point on a particular i-level at $t = \Delta t$. Similarly the values of T are calculated from Eq. (14). Using the values of C and T in Eq. (13), values of U are calculated. Then the values of V are calculated explicitly by using Eq. (12) at every nodal point on a particular i-level. After computing values corresponding to each i at a time level, the values at the next time level are determined similarly. Computations are repeated until the steady state is reached. The steady-state solution is assumed to have been reached when the absolute difference between values of velocity U, temperature T as well as concentration C at two consecutive time steps are less than 10^{-5} at all grid points.

After experimenting with few set of mesh sizes, the mesh sizes have been fixed at the level $\Delta X = 0.02$, $\Delta R = 0.2$, with time step $\Delta t = 0.01$. In this case, spatial mesh sizes are reduced by 50% in one direction, and later in both directions, and results are compared. It is observed that, when the mesh size is reduced by 50% in the R-direction, the results differ in the fifth place while the mesh sizes are reduced by 50% in X-direction or in both directions the results are correct to fourth decimal place. Hence, the above mesh sizes have been considered as appropriate.

5
Results and discussion

The transient velocity profiles for different values of the Schmidt number, the Prandtl number, and the thermal Grashof number and mass Grashof number are shown in Fig. 1. The velocity profiles presented are those at $X = 1.0$. It is observed that the velocity slowly increases with time, reaches a temporal maximum around time $t = 0.77$ and becomes steady at time $t = 7.44$. It also observed that the velocity increases with increasing values of Gr and Gc and

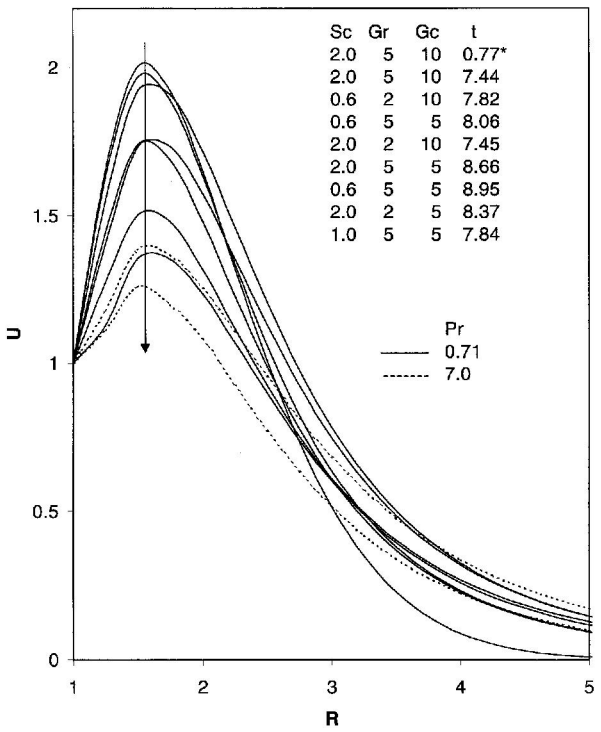

Fig. 1. Transient velocity profiles at $X = 1.0$. *temporal maximum

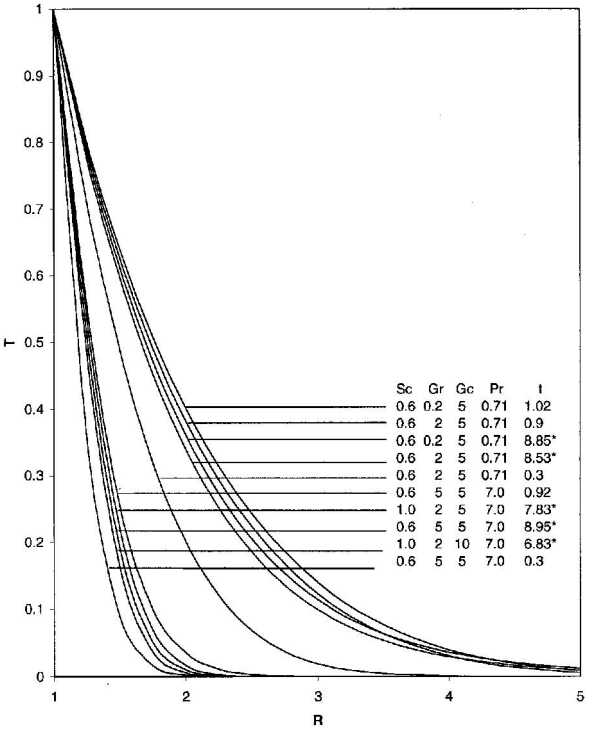

Fig. 2. Transient temperature profiles at $X = 1.0$. *Steady state

decreasing values of Sc. The contribution of mass diffusion to the buoyancy force increases the maximum velocity significantly.

The transient temperature profiles for different Gr, Gc, Sc and Pr is plotted in Fig. 2. It is known that Pr plays an important role in flow phenomena because it is a measure of the relative magnitude of viscous fluid boundary layer thickness to the thermal boundary layer thickness. The thermal boundary layer thickness decreases with increasing values of Pr. It is observed that temperature decreases with increasing values of Gr or Gc. The time taken to reach the steady state increases with decreasing values of Sc, Gr and Gc when Pr is high. The temporal maximum is also shown in Fig. 2 around the time $t = 1.02$ and becomes steady state $t = 8.85$.

The concentration profiles for different Schmidt numbers are shown in Fig. 3. It is observed that the concentration is increasing with decreasing values of Schmidt number. The time taken to reach the steady state increases with decreasing values of Sc. The transient concentration profiles for different values of Gr and Gc are shown in Fig. 4. It is clear that the concentration increases with decreasing values of Gr or Gc.

Knowing the numerical values of velocity, concentration, we now calculate the local and average skin-friction, the rate of heat transfer and mass transfer both in the transient and steady state conditions. The local as well as average skin-friction, Nusselt number and Sherwood number in terms of dimensionless quantities are given by

$$\tau_x = -(\partial U/\partial R)_{R=1} \tag{16}$$

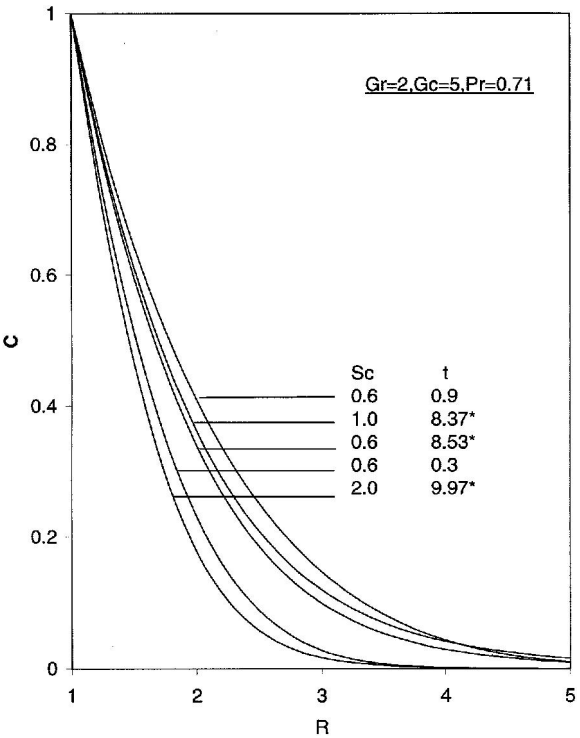

Fig. 3. Transient concentration profiles at $X = 1.0$ for different Sc. *Steady state

$$\bar{\tau} = -\int_0^1 (\partial U/\partial R)_{R=1} \mathrm{d}X \tag{17}$$

$$\mathrm{Nu}_x = -X(\partial T/\partial R)_{R=1} \tag{18}$$

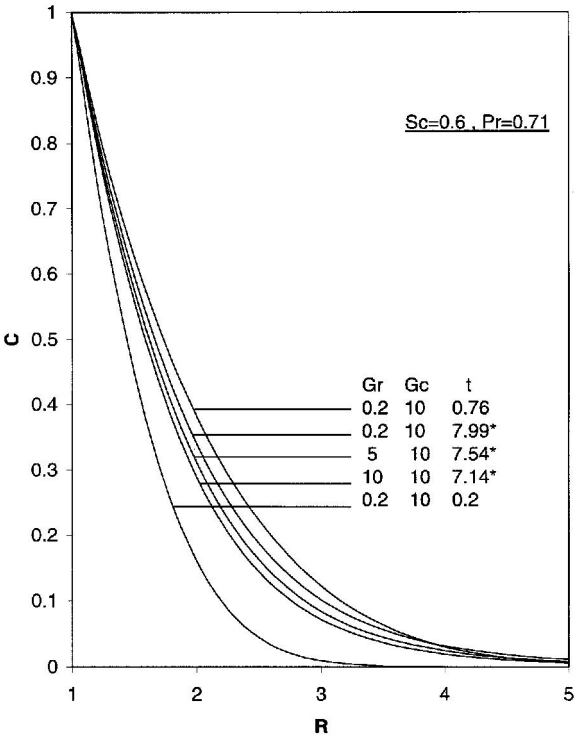

Fig. 4. Transient concentration profiles at $X = 1.0$ for different Gr and Gc. *Steady state

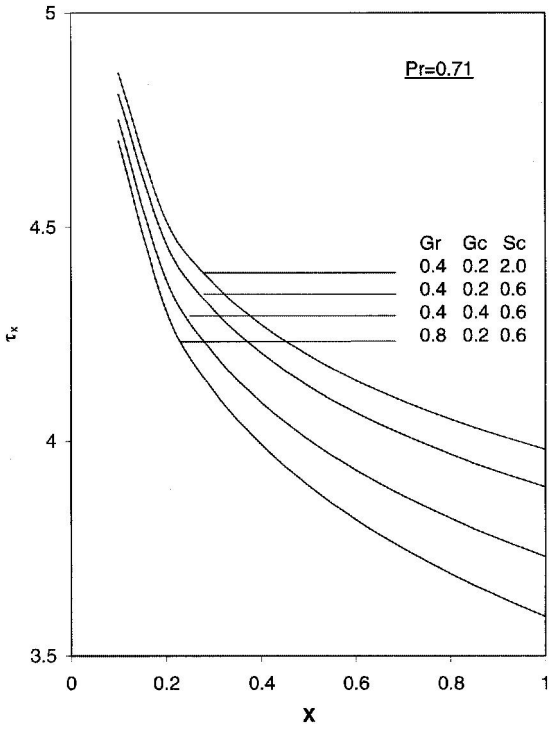

Fig. 5. Local skin-friction

$$\overline{\mathrm{Nu}} = -\int_0^1 [(\partial T/\partial R)_{R=1}]\mathrm{d}X \tag{19}$$

$$\mathrm{Sh}_x = -X(\partial C/\partial R)_{R=1} \tag{20}$$

$$\overline{\mathrm{Sh}} = -\int_0^1 [(\partial C/\partial R)_{R=1}]\mathrm{d}X \tag{21}$$

These derivatives involved in the Eqs. (16)–(21) are evaluated using five-point approximation formula and integrals are evaluated using Newton–Coats formula.

The local skin frictions are plotted in Fig. 5. It is observed that the local skin-friction decreases as X increases. The local wall shear stress increases with decreasing values of Gr or Gc. It is observed that there is fall in skin friction due to decreasing Sc. The local Nusselt number for different Gr, Gc and Sc are shown in Fig. 6. The local Nusselt number increases with decreasing values of Sc and increases with increasing Gr or Gc. This trend is just opposite in local Sherwood number with respect to the Sc because the concentration profiles decreases with increasing values of Sc, near the cylinder as shown in Fig. 7.

The effect of Gr, Gc and Sc on the average values of skin friction, Nusselt number and Sherwood number are shown in Fig. 8–10, respectively. The average skin friction increases with decreasing values of Gr or Gc throughout the transient period. The Nusselt number increases with decreasing Sc and it increases with increasing Gr or Gc. The average Sherwood number increases with increasing Schmidt number.

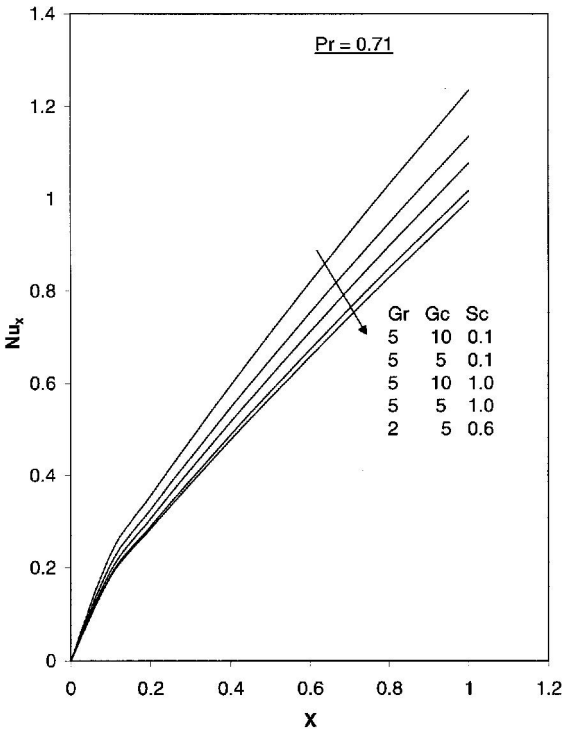

Fig. 6. Local Nusselt number

6 Conclusion

1. The time required to reach the steady in velocity and temperature is more when Pr is high. Time taken to reach the steady increases as Gr decreases.

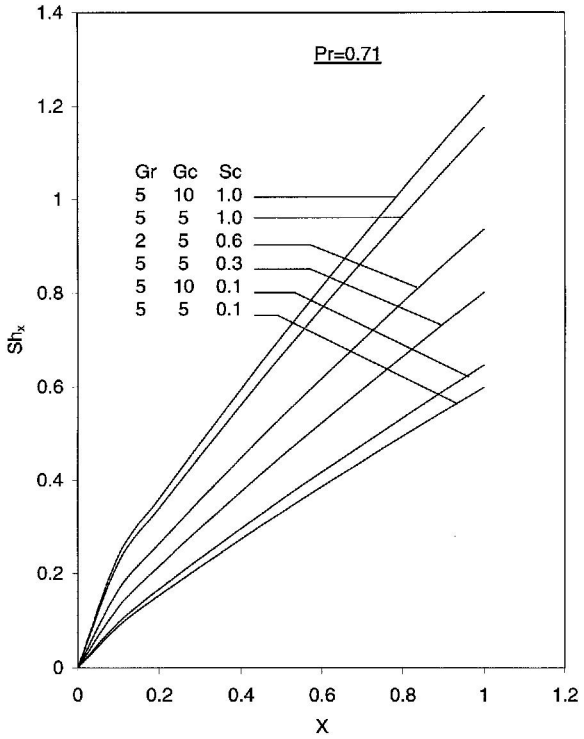

Fig. 7. Local Sherwood number

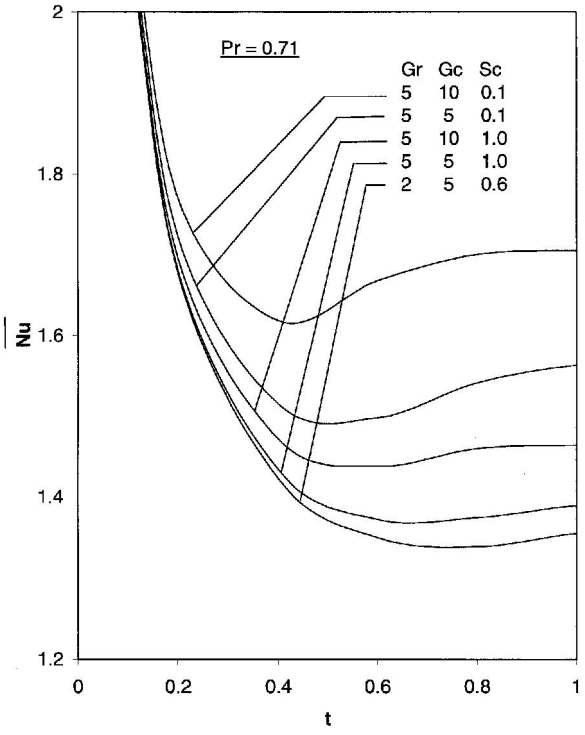

Fig. 9. Average Nusselt number

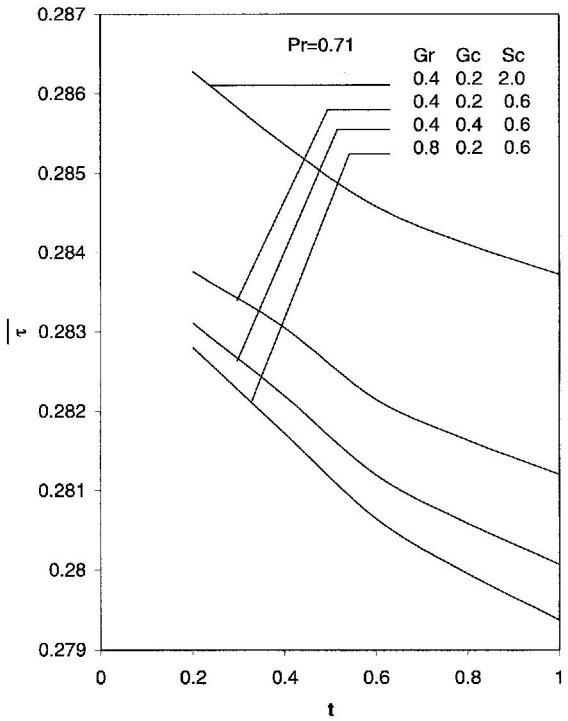

Fig. 8. Average skin-friction

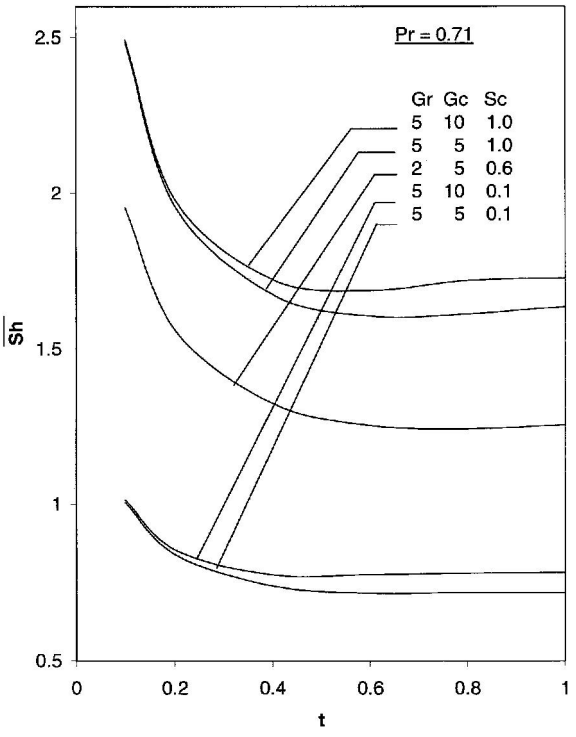

Fig. 10. Average Sherwood number

2. The skin friction values are negative at small values of the Sc, i.e., there may occur separation near the cylinder, but with large values of Sc, the skin friction values are positive indicating that there may not occur separation of the flow at the cylinder. The shearing stress increases with increasing value of Pr and decreasing values of Gr.

3. The rate of heat transfer increases with increasing values of Pr and Gr or Gc and decreasing values of Sc.

4. The mass of heat transfer is found to become more effective as the thermal buoyancy force increases. While the local surface heat transfer is enhanced as the Schmidt number is decreased, the surface mass transfer increases with increasing Schmidt number.